Investigation of the Inner Nozzle Wake on Kelvin Helmholtz Instabilities in a Coannular Jet

Shekhar Sarpotdar* and Ganesh Raman†
Fluid Dynamics Research Center, Illinois Institute of Technology, Chicago, IL-60616, USA

ABSTRACT

In the present work, we study stability characteristics of synthetic profiles prototypical of coannular jets, using a spatial, inviscid and compressible formulation of linear stability theory. The focus of our study is to understand the effect of the wake of the nozzle that separates the primary jet from the secondary jet, on the characteristics of different instability modes. Some of the parameters under focus are Mach number of the primary jet (M_1), wake deficit (W_{amp}), and temperature ratio (T_{01}/T_∞). One of the other aims of this work is to compare our results with that of the 2-D planar mixing layers separated by a splitter plate – for which counteracting effect of compressibility and the wake of the splitter plate, on the instability characteristics, are known. Our results show that, for circular jets, unlike 2-D planar mixing layers, the vorticity introduced by the wake fails to overcome the stabilization effect caused by compressibility. Heating the jet, i.e., increasing the temperature ratio T_{01}/T_∞, may increase or decrease the maximum growth rate depending on the exact combination of the flow parameters and the particular stability mode.

1. INTRODUCTION

Noise emitted from aircraft is one of the major causes that impose constraints on the maximum utilization of airports and air transportation. Aircraft companies have been researching novel noise reduction concepts. Engines with a high bypass ratio, wherein a high speed stream of air from the main jet is shrouded by a low speed coannular jet, is one such concept. Although the concept is successful and has been integrated with real jet engines, it is still an area of active research and development. Researchers have been trying to improve nozzle contours [1] and understand noise sources associated with these jet flows through experiments and computations.

Based on the nozzle that carries the high velocity stream of air, coannular jet flows can be divided into two categories, i.e., Normal Velocity Profile (NVP) coannular jets and Inverted Velocity Profile (IVP) coannular jets. In the case of NVP, it is the inner nozzle that carries high velocity stream, whereas in the case of IVP, the outer coannular nozzle carries high speed stream of air. Out of these two configurations the NVP configuration is more common. Figure 1 shows a schematic of the flow field of a typical NVP coannular jet. As the high speed *primary* jet and annular low speed *secondary* jet of air leave the inner nozzle and outer nozzle respectively, they form their individual potential cores. Between these two potential cores, lies an annular wake of the inner nozzle. Note that this wake is not only generated due to the flow obstructed by the nozzle lip, but also due to the boundary layer that develops on both the sides of the nozzle. To the best of our knowledge the effect of the wake of the nozzle has not been examined systematically, in the compressible regime. Such an analysis is useful for high speed jet flows, since for the planar shear layers, the wake effect is known to counteract the compressibility effect, i.e., increasing the Mach number reduces the shear layer growth rate, but adding wake into the shear layer profile increases its growth rate [2]. It is the influence of this wake on the stability characteristics of the NVP jet that is a focus of this study. Such study would be useful designing coannular jet nozzles for applications ranging from industrial burners to jet engines.

Stability of circular jets has been the subject of interest for a long time. With the advent of jet engines – and the noise produced by them becoming a growing concern – the subject gained practical importance and more attention. Knowledge of stability characteristics is critical to understanding the

*Electronic address: sarpshe@iit.edu

†Electronic address: Raman@iit.edu

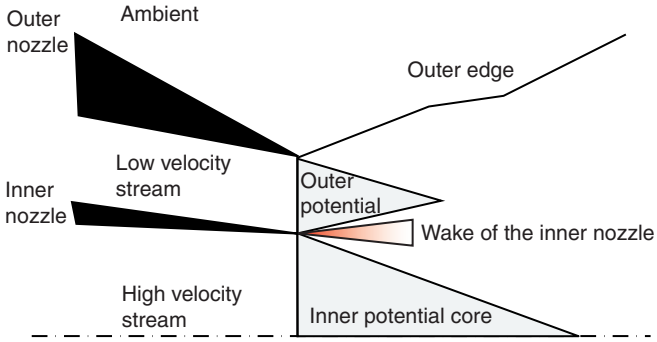

Figure 1. Schematic of the flow field of the Normal Velocity Profile (NVP) coannular jet.

development of large scale turbulent structures which influence aeroacoustic properties of high speed shear layers and jets [3]. Michalke [4] was one of the first ones to review the theoretical work done in this area. He reviewed spatial stability of both parallel flow and slowly diverging circular jet flows. His focus was mainly on subsonic circular jets. In a series of experimental studies Oertel [5] observed three families of waves, viz., subsonic instability, supersonic instability and Kelvin Helmholtz Instability; each with its own distinct characteristic and phase speed. Tam and Hu [6] showed the existence of these three types of instabilities analytically. They also specified criteria for the individual instability, using linear stability theory. They found that for these instabilities to occur, the jet must be supersonic in the instability wave frame of reference. Panickar and Raman [7, 8] performed linear stability analysis relevant to the problem of jet impingement tones and its control. Thurow et al. [9, 10] performed experimental study to measure the convective velocity of large scale structures in the circular mixing layers of high speed jet.

Villermaux and Rehab [11] and Rehab et al. [12] provided a very detailed account of near field flow structures of a coaxial jet. Rehab et al. [12] found that for large velocity ratio, the stability mechanism of an IVP type jet may depart from common convective spatial stability to the that of the absolute stability associated with the back flow within the inner jet.

Dahm et al. [13] performed experimental work, by changing the velocity of the low speed and high speed stream, to shed light on the stability of the coannular jets. They supplemented this experimental study with numerical analysis. However, their study was limited to low Reynolds numbers, where compressibility was unimportant. Dahl and Morris [14, 15] performed a rigorous investigation of the coannular jets at high Mach numbers. They analytically calculated the mean flow field and then used it to predict the aeroacoustic characteristics of the jet. However, they did not take into account the wake of the inner nozzle in their analysis.

Fang and Reshotko [16] and Michalke [17] were one of the few, who investigated the instability of wake dominated mixing layers. However, they restricted their study to the single stream nozzle configuration – with specific focus on the flight effect. In the present study the configuration is that of the coannular jet velocity profiles, in which the interface of primary and secondary jets contains velocity deficit due to the wake of the inner nozzle. We especially focus on the effect of compressibility and heating of these jets.

2. METHODOLOGY

2.1. Linear Stability Analysis

In this section we develop the stability equations within the framework of linear stability theory as applied to the compressible, inviscid, nearly parallel axisymmetric flows in radial coordinates. Adhering to the cylindrical (x, r, θ) coordinate system, we now list the governing equations. The continuity equation is given by:

$$\frac{\partial \rho}{\partial t} + \frac{1}{r}\frac{\partial \left(\rho r v\right)}{\partial r} + \frac{1}{r}\frac{\partial \left(\rho w\right)}{\partial \theta} + \frac{\partial \left(\rho u\right)}{\partial x} = 0, \tag{1}$$

Where u, v and w are the velocity components in x, r and θ direction respectively and ρ is the fluid density. The momentum equations in x, r and θ direction are as follows.

$$\rho\left[\frac{\partial u}{\partial t}+v\frac{\partial u}{\partial r}+\frac{w}{r}\frac{\partial u}{\partial \theta}+u\frac{\partial u}{\partial x}\right]+\frac{\partial p}{\partial x}=0, \tag{2}$$

$$\rho\left[\frac{\partial v}{\partial t}+v\frac{\partial v}{\partial r}+\frac{w}{r}\frac{\partial v}{\partial \theta}-\frac{w^2}{r}+u\frac{\partial v}{\partial \theta}\right]+\frac{\partial p}{\partial r}=0, \tag{3}$$

$$\rho\left[\frac{\partial w}{\partial t}+v\frac{\partial w}{\partial r}+\frac{w}{r}\frac{\partial w}{\partial \theta}+\frac{vw}{r}+u\frac{\partial w}{\partial x}\right]+\frac{1}{r}\frac{\partial p}{\partial \theta}=0, \tag{4}$$

The energy equation, for ideal gas with constant specific heats in the absence of heat exchange and body forces, is given by:

$$\frac{\partial p}{\partial t}+v\frac{\partial p}{\partial r}+\frac{w}{r}\frac{\partial p}{\partial \theta}+u\frac{\partial p}{\partial x}+\gamma p\left[\frac{1}{r}\frac{\partial (vr)}{\partial r}+\frac{1}{r}\frac{\partial w}{\partial \theta}+\frac{\partial u}{\partial x}\right]=0, \tag{5}$$

Note that the above equations are in nondimensional form. The density ρ^* has been nondimensionalized using primary jet centerline density at the nozzle exit, ρ_1^*, i.e., $\rho = \rho^*/\rho_1^*$. Here superscript '*' denotes that the the quantity is in dimensional form. The subscript '1' refers to the property at the centerline of the primary jet. The velocity $\mathbf{u}^* = (u^*, v^*, w^*)$ has been nondimensionalized using primary jet centerline velocity u_1^*. The pressure has been nondimensionalized using $\rho_1^* u_1^{*2}$, and the lengths are nondimensionalized using the radius of the primary jet at the exit, i.e., r_I^*. Here, the subscript 'I' refers to the inner nozzle perimeter. Similarly, whenever subscript 'II' is used, it refers to the outer nozzle perimeter. Next, assuming the flow to be locally parallel, the density, ρ, the pressure, p, and the velocity components, u, v and w are decomposed into mean and fluctuating/perturbation terms as shown below:

$$u\Big(x,r,\theta,t\Big)=\overline{u}(r)+\tilde{u}(x,r,\theta,t), \tag{6}$$

$$v\Big(x,r,\theta,t\Big)=\tilde{v}(x,r,\theta,t), \tag{7}$$

$$w\Big(x,r,\theta,t\Big)=\tilde{w}(x,r,\theta,t), \tag{8}$$

$$p\Big(x,r,\theta,t\Big)=\overline{p}+\tilde{p}(x,r,\theta,t), \tag{9}$$

$$\rho\Big(x,r,\theta,t\Big)=\overline{\rho}(r)+\tilde{\rho}(x,r,\theta,t). \tag{10}$$

where terms with an overbar denote the mean part and those with a tilde denote the fluctuating part of the given variable. The mean pressure which is equal to the ambient pressure, is assumed to be uniform at any given cross section of the jet.

Substituting the decompositions given in (6)–(10) into (1) to (5), and eliminating terms that contain the product of fluctuating terms, the linearized equations governing the perturbation quantities can be written as follows:

$$\frac{\partial \tilde{\rho}}{\partial t}+\frac{1}{r}\frac{\partial\left(\overline{\rho} r\tilde{v}\right)}{\partial r}+\frac{1}{r}\frac{\partial\left(\tilde{w}\right)}{\partial \theta}+\overline{\rho}\frac{\partial\left(\overline{u}\right)}{\partial x}+\overline{u}\frac{\partial \tilde{\rho}}{\partial x}=0, \tag{11}$$

$$\overline{\rho}\left[\frac{\partial \overline{u}}{\partial t}+\tilde{v}\frac{\partial \overline{u}}{\partial r}+\overline{u}\frac{\partial \overline{u}}{\partial x}\right]+\frac{\partial \tilde{p}}{\partial x}=0, \tag{12}$$

$$\overline{\rho}\left[\frac{\partial \tilde{v}}{\partial t}+\overline{u}\frac{\partial \tilde{v}}{\partial x}\right]+\frac{\partial \tilde{p}}{\partial r}=0, \tag{13}$$

$$\overline{\rho}\left[\frac{\partial \tilde{w}}{\partial t}+\overline{\rho}\,\overline{u}\frac{\partial \tilde{v}}{\partial x}\right]+\frac{1}{r}\frac{\partial \tilde{p}}{\partial \theta}=0, \tag{14}$$

$$\frac{\partial \tilde{p}}{\partial t}+\overline{u}\frac{\partial \tilde{p}}{\partial x}+\gamma\overline{p}\left[\frac{1}{r}\frac{\partial(\tilde{v}r)}{\partial r}+\frac{1}{r}\frac{\partial \tilde{w}}{\partial \theta}+\frac{\partial \tilde{u}}{\partial x}\right]=0, \tag{15}$$

where $\gamma\overline{p}=\dfrac{1}{M_j^2}$ which follows form the laws of ideal gas.

The linearized equations show that the perturbation density term, $\tilde{\rho}$ occurs only in the continuity equation. Equation (11) thus decouples from the momentum and energy equations. Hence, only equations (12)–(15) need to be considered. Substituting the normal-mode ansatz given by:

$$\left[\tilde{u},\tilde{v},\tilde{w},\tilde{p}\right]=\left[\hat{u}(r),\hat{v}(r),\hat{w}(r),\hat{p}(r)\right]e^{i(\alpha x+n\theta-\omega t)} \tag{16}$$

into equations (12)–(15), a coupled system of ordinary differential equations for $\hat{u}(r),\ \hat{v}(r),\ \hat{w}(r)$ and $\hat{p}(r)$ is obtained. This coupled system can be solved to yield a single equation in the variable of interest, in this case the perturbation pressure, $\hat{p}$, as follows:

$$\frac{d^2\hat{p}}{dr^2}-\left\{\frac{1}{r}-\frac{1}{\overline{\rho}}\frac{d\overline{\rho}}{dr}+\frac{2\alpha}{\omega-\alpha\overline{u}}\frac{d\overline{u}}{dr}+\right\}\frac{d\hat{p}}{dr}+\left\{M_1^2\overline{\rho}(\omega-\alpha\overline{u})^2-\frac{n^2}{r^2}-\alpha^2\right\}\hat{p}=0. \tag{17}$$

Equation (17) is the two-dimensional, compressible Rayleigh equation [4]. To solve this equation using the shooting method, we cast this equation in the form of phase velocity eigenvalue problem, i.e., we substitute c for α in (Equation (17)).

$$\frac{d^2\hat{p}}{dr^2}-\left\{\frac{1}{r}-\frac{1}{\overline{\rho}}\frac{d\overline{\rho}}{dr}+\frac{2}{c-\overline{u}}\frac{d\overline{u}}{dr}+\right\}\frac{d\hat{p}}{dr}+\left\{M_1\omega^2\overline{\rho}\left(1-\frac{\overline{u}}{c}\right)^2-\frac{n^2}{r^2}-\alpha^2\right\}\hat{p}=0. \tag{18}$$

Equation (18) is the phase velocity form of the Rayleigh equation. Solving the equation for complex phase velocity c instead of α gives better numerical performance. This is due to the fact that, for a given ω, the possible range of real α values is far greater than the possible range of c values. This is partly due to the fact that the real part of c lies within the bounds of maximum and minimum velocities in the flow [15].

In Equation (18) instead of computing or experimentally measuring the mean velocity $\bar{u}$ we resort to artificial velocity profiles, referred to as *synthetic* profiles, prototypical of the ones obtained just at the exit of the coannular nozzles. The equation for the synthetic profiles is

$$\bar{u}(r) = (1-h)\,\bar{u}_I + h\bar{u}_{II} - W_{amp}\exp\left[-\left(\frac{r - W_{off}}{W_{wid}}\right)^2\right] \tag{19}$$

where

$$\bar{u}_n(r) = \frac{1}{2}\left[1 + tan\,h\left[b_n\left(\frac{r_n}{r} - \frac{r}{r_n}\right)\right]\right], n = I, II, b_n = \frac{r_n}{4\theta_n} = r_n\,\delta_\omega \tag{20}$$

The above equations are adapted from the work of Perrault-Joncas and Maslowe [18]. In this equation θ, δ_ω, W_{amp}, W_{off} and W_{wid} represent relative strength of two shear layer momentum thickness, vorticity thickness, wake amplitude, wake offset and wake width respectively. The equation is a combination of two hyperbolic tangent profiles and a Gaussian distribution. One of the hyperbolic tangent profiles simulates the mixing layer between the primary jet and secondary stream, whereas the other one simulates the mixing layer between secondary stream and the ambient. The Gaussian distribution part of the velocity profile simulates the wake of the inner nozzle, that separates the primary jet and secondary stream. Figure 2 shows sample synthetic velocity profile along with their spatial derivative for different values of W_{amp}, viz., 0, 0.2, 0.5, and 0.7. The values of other parameters of these synthetic profiles are as follows: h = 0.7, θ_I = 0.1, θ_{II} = 0.14, $\frac{r_{II}}{r_I}$ = 2, W_{amp} = 0.1, W_{off} = 1. In Fig. 2b the arrows denote inflection points in the velocity profiles. As seen in the figure, a typical synthetic profile consists of three inflection points. Each inflection point is found to be associated with one instability mode.

Flows for which pressure at any given cross section is constant, and $Pr \approx 1$, density can be found using Crocco relation [4, 19]:

$$\bar{\rho} = \frac{1}{\bar{T}} = \left[\frac{1}{2}(\gamma - 1)(1 - \bar{u})\,\bar{u}M_1^2 + \bar{u} + 1 + \frac{\bar{T}_\infty}{\bar{T}_1}(1 - \bar{u})\right]^{-1}. \tag{21}$$

where

$$\frac{T_\infty}{T_1} = \frac{T_\infty}{T_{01}}\left[1 + \frac{\gamma - 1}{2}M_1^2\right] \tag{22}$$

Here subscript '0' refers to the stagnation condition.

Next, the boundary conditions required to solve (17) need to be discussed. Along the centerline of the jet, $\bar{u} = \bar{\rho} = 1$ and $\bar{u}' = \bar{\rho}' = 0$, where '′' denotes differentiation in the radial direction. At sufficiently large distance away from the jet, i.e., $r \to \infty$, $u = 0$, $\bar{\rho} = T_1/T_\infty$ and $\bar{u}' = \bar{\rho}' = 0$. These conditions fix the value of the pressure eigenfunction at the boundary through Bessel and Hankel function. Interested readers are referred to the work of Panickar and Raman [14] for further details.

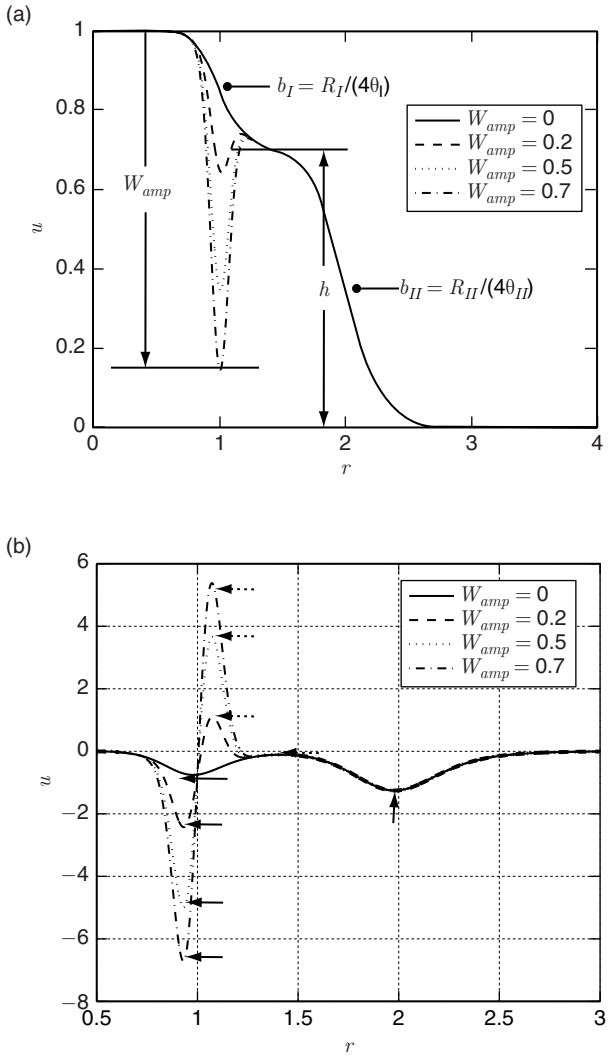

Figure 2. Sample synthetic velocity profiles described by equation 19 for different values W_{amp} and h = 0.7, θ_I = 0.1, θ_{II} = 0.14, $\frac{R_{II}}{R_{Is}}$ = 2, W_{off} = 1. (a) Profiles of u(r); (b) profiles of $\frac{du(r)}{dr}$. The arrows in the part 'b' of the figure indicate inflection points.

3. COLD JETS

We now investigate the influence of different parameters on the characteristics of Kelvin-Helmholtz type instabilities. Figure 3 shows typical pressure eigenfunctions of different instability modes associated with different inflection points in the velocity profiles. Each subfigure shows two eigenfunctions, one for the axisymmetric (n = 0) mode and one for the helical mode (n = 1). Figure 3a shows eigenfunctions of the instability modes associated with the inflection point along the interface between the primary jet and the secondary jet. We refer to this mode as 'Shear Layer Mode I'. Figure 3b shows the eigenfunctions associated with the inflection points along the the interface between the secondary jet and the ambient. We refer to it as 'Shear Layer Mode II'. In Fig. 2b one can see that the wake of the inner nozzle gives rise to an additional inflection point along the interface between the primary jet and the secondary jet. We refer to the eigenfunctions associated with this inflection point as 'Wake Mode I'. Note that eigenfunctions associated with Wake Mode I have a double peak shape at the inflection point (see Fig. 3c), unlike Shear Layer Mode I and Shear Layer Mode II, which have a single peak at their respective inflection points. One can see that all the axisymmetric mode (n = 0) eigenfunctions have finite

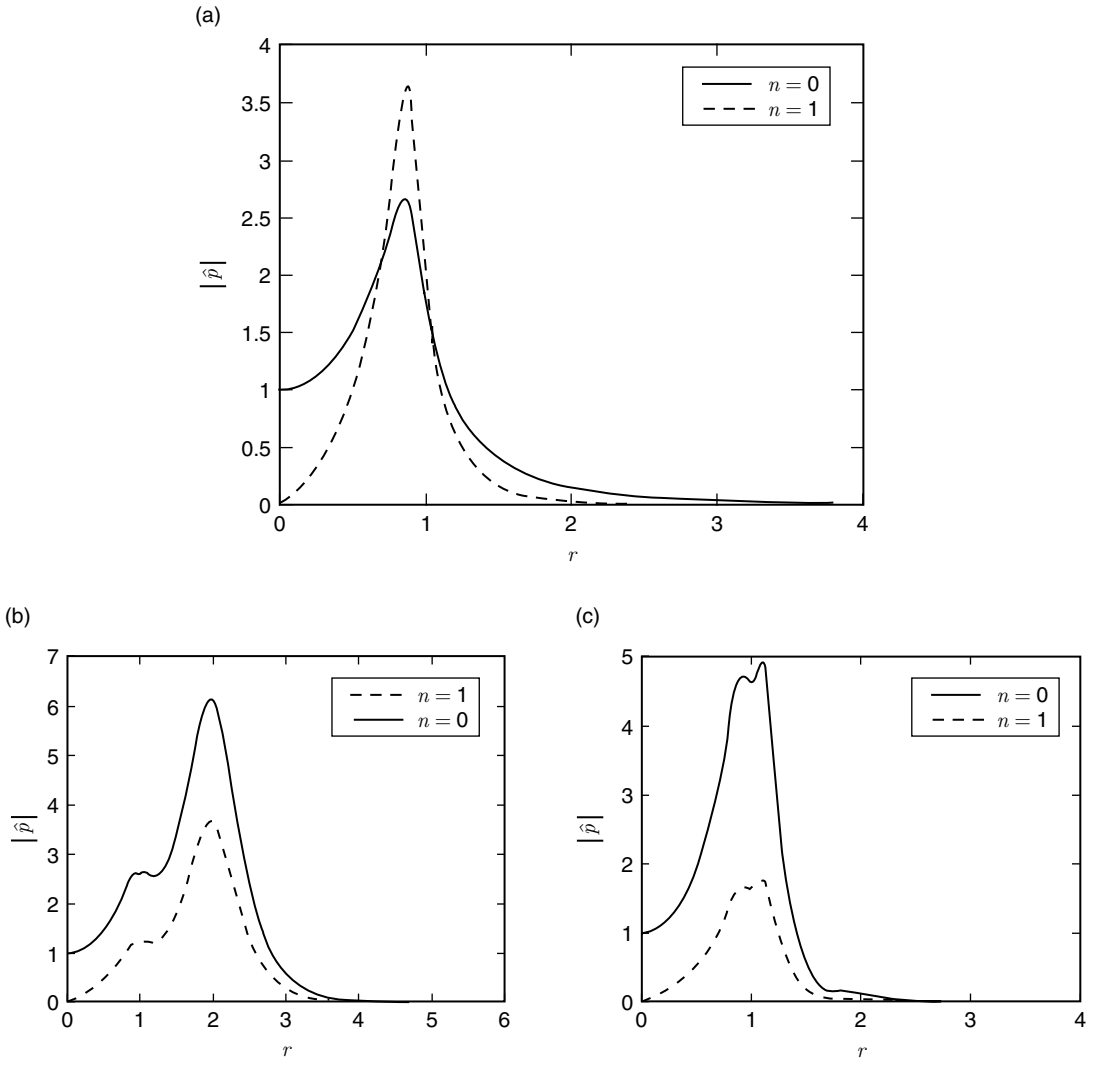

Figure 3. Three pressure eigenfunctions, each associated with different inflection point along the velocity profiles, investigated in the present study, (a) Eigenfunction for the Shear Layer Mode I; (b) Eigenfunction for the Shear Layer Mode II and (c) Eigenfunction for the Wake Mode I.

amplitude at the center of the jet. Whereas, the pressure amplitude of the helical mode (n = 1) eigenfunctions becomes zero at the center of the jet.

We first evaluate the influence of W_{amp} on the instability characteristics of Shear Layer Mode I, Shear Layer Mode II and Wake Mode I for n = 0, i.e., axisymmetric mode. Figure 4 shows the influence of W_{amp} on the growth rate of Shear Layer Mode I (Fig. 4a), Shear Layer Mode II (Fig. 4b) and Wake Mode I (Fig. 4c). One can see that introduction of the wake, with increasing wake deficit (W_{amp}) has a strong destabilizing effect on Shear Layer Mode I. Increasing W_{amp} increases both maximum growth rate and range of unstable frequencies. For the synthetic profile with W_{amp} = 0.6, the maximum growth rate has increased by an order of magnitude. For smaller values of W_{amp}, the range of unstable frequencies grows very fast with increase in W_{amp}. However, increasing W_{amp} beyond 0.4 does not increase the range of unstable frequencies. Introduction of the wake increases the growth rate of Shear Layer Mode II too. However, compared to Shear Layer Mode I the impact of the wake on Shear Layer Mode II appears to be very marginal. Figure 4c shows the influence of the wake on the growth rates of Wake Mode I. One can see that as the wake deficit (W_{amp}) reduces, so does the maximum growth rate of Wake Mode I. Note that as the wake diminishes, the maximum growth rate approaches zero, i.e.,

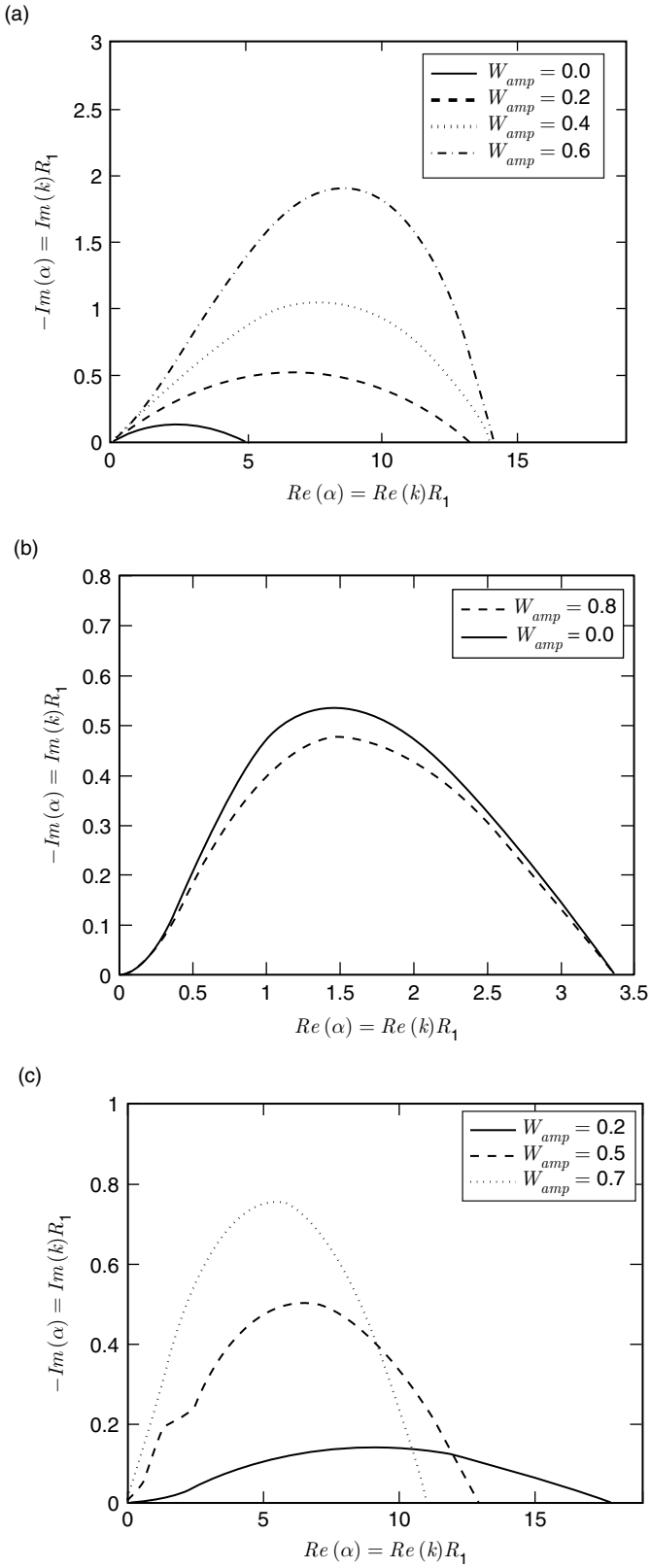

Figure 4. Influence of the W_{amp} on the spatial growth rate of (a) Shear Layer Mode I; (b) Shear Layer Mode II and (c) Wake Mode I.

$W_{amp} \rightarrow 0 \Rightarrow -Im(\alpha) \rightarrow 0$. Reduction in the maximum growth rate is accompanied by an increase in the range of unstable frequencies. Figure 5 shows phase velocities of the corresponding cases shown in Fig. 4. Increasing W_{amp} is found to reduce the phase velocity of Shear Layer Mode I and Wake Mode I. However, for Shear Layer Mode I the effect is visible only at higher wavenumbers, whereas for Wake Mode I it is consistent across all wavenumbers. The wake deficit (W_{amp}) seems to have very little effect on the phase velocity of Shear Layer Mode II.

We now evaluate the effect of compressibility, i.e., Mach number, on the stability characteristics of Shear Layer Mode I, Shear Layer Mode II and Wake Mode I. We use the W_{amp} = 0.7 profile with $\frac{T_{01}}{T_{\infty}}$ shown in Fig. 2 for our study. Figures 6 and 7 show the influence of compressibility on the growth rate and phase velocity respectively. One can see that increasing the Mach number reduces the maximum growth rate of both Shear Layer Mode I (Fig. 6a) and Shear Layer Mode II (6b). Note that for both the shear layer modes, by increasing the Mach numbers up to 1.5, the range of unstable frequency reduces. However, above Mach number 1.5, the range of unstable frequency slightly increases. In the case of Wake Mode I, up to Mach number 1, the maximum growth rate and the range of unstable frequencies reduce. However, above Mach number 1.0, both maximum growth rate and the range of unstable frequencies start to grow. As far as the phase speed is concerned, in Figs. 7a and 7b one can see that, for both shear layer modes up to Mach number 1.5, the change in the phase speed is marginal. However, above Mach number 1.5, increasing the Mach number significantly increases the phase speed.

At this point we would like to mention that, for unbounded 2-D planar mixing layers as per linear stability theory compressibility provides a stabilization effect [20, 21], i.e., by increasing the Mach number the maximum growth rate of the mixing layers approaches zero. However, experimental

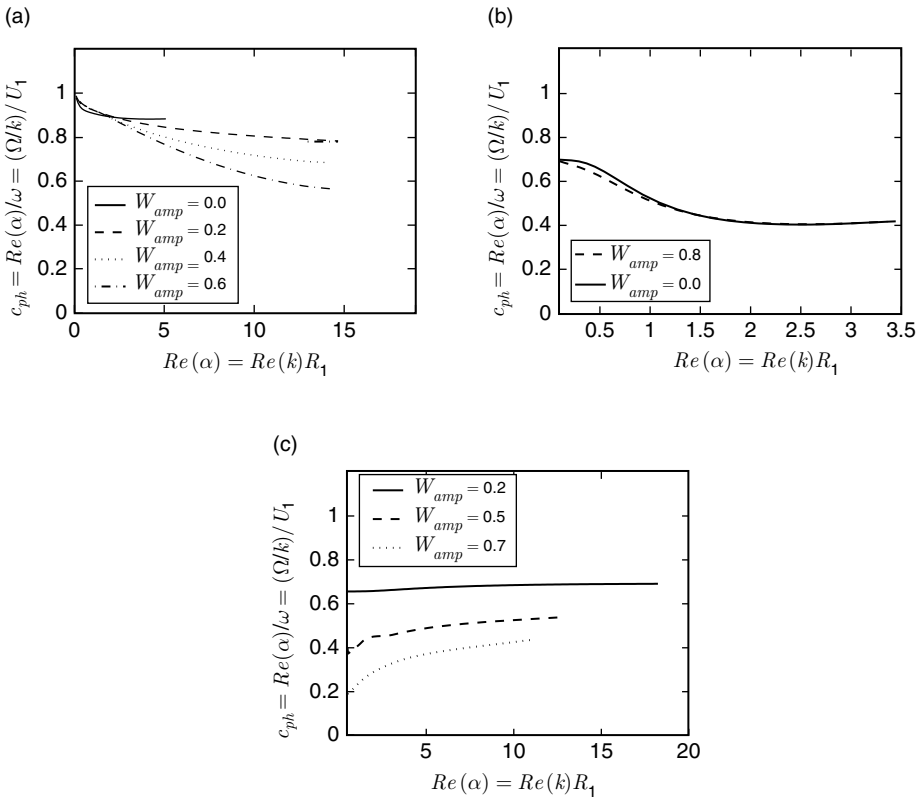

Figure 5. Influence of the W_{amp} on the spatial phase velocity of (a) Shear Layer Mode I; (b) Shear Layer Mode II and (c) Wake Mode I.

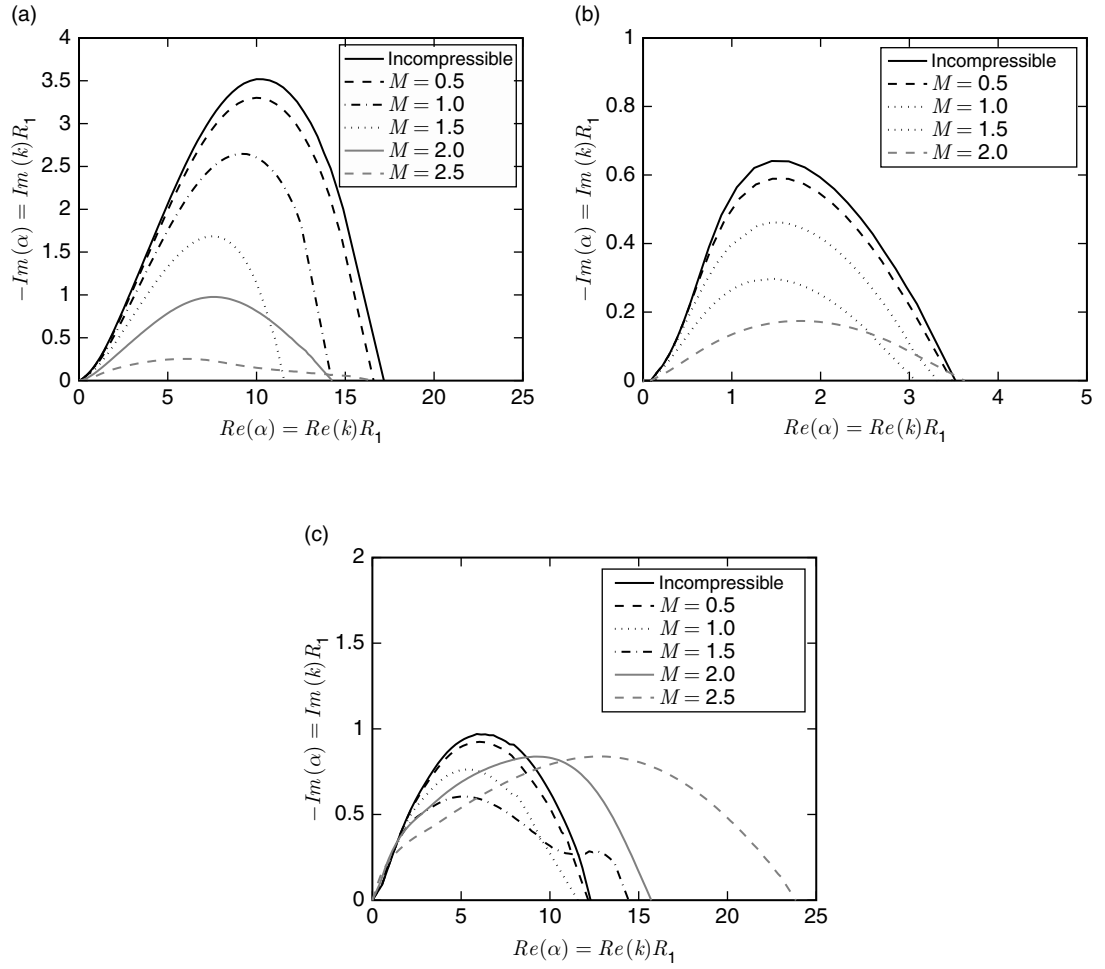

Figure 6. Influence of the Mach number on the spatial growth rate of (a) Shear Layer Mode I; (b) Shear Layer Mode II and (c) Wake Mode I.

evidence has shown that, even at very high Mach numbers the shear layer growth rates do not fall below a minimum growth rate [22]. Dimotakis and Zhuang [2] addressed this discrepancy using linear stability analysis of the wake dominated mixing layers. They found that the wake of the splitter plate that separates the low speed stream from the high speed stream, provides a strong destabilization effect. Figure 5a in their work shows that, for pure mixing layers – without wake – the maximum growth rates become zero at sufficiently high Mach number. However, for the wake dominated mixing layers this is not the case. The presence of the wake counteracts the stabilization effect provided by the compressibility and prevents the mixing layers to become stable at high Mach numbers.

Figure 8 sheds light on the counteracting effect of compressibility and the wake of the inner nozzle for Shear Layer Mode I (Fig. 8a) and Wake Mode I (Fig. 8b) of coannular jets. In Fig. 8a the destabilizing effect of the wake on Shear Layer Mode I is evaluated for W_{amp} ranging from 0 to 0.7. In this figure, for the case W_{amp} = 0, increasing the Mach number, the maximum growth rates monotonically approach zero – similar to 2-D planar mixing layers. However, for the wake dominated radial mixing layers (cases for which $W_{amp} > 0$) the counteracting effect of wake against compressibility is different from the 2-D planar mixing layer. Unlike wake dominated planar mixing layers, in the case of wake dominated radial mixing layers, the wake fails to counteract the stabilization

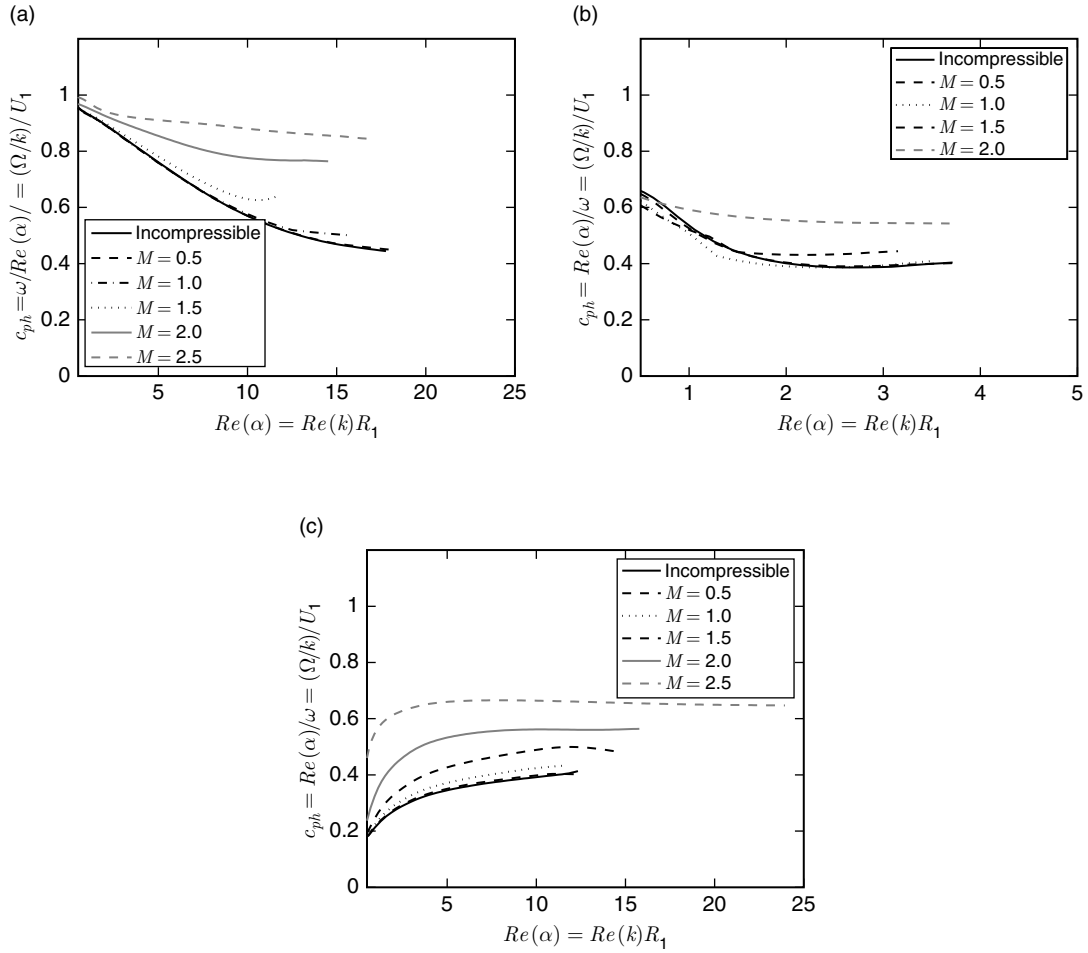

Figure 7. Influence of the Mach number on the phase velocity of (a) Shear Layer Mode I; (b) Shear Layer Mode II and (c) Wake Mode I.

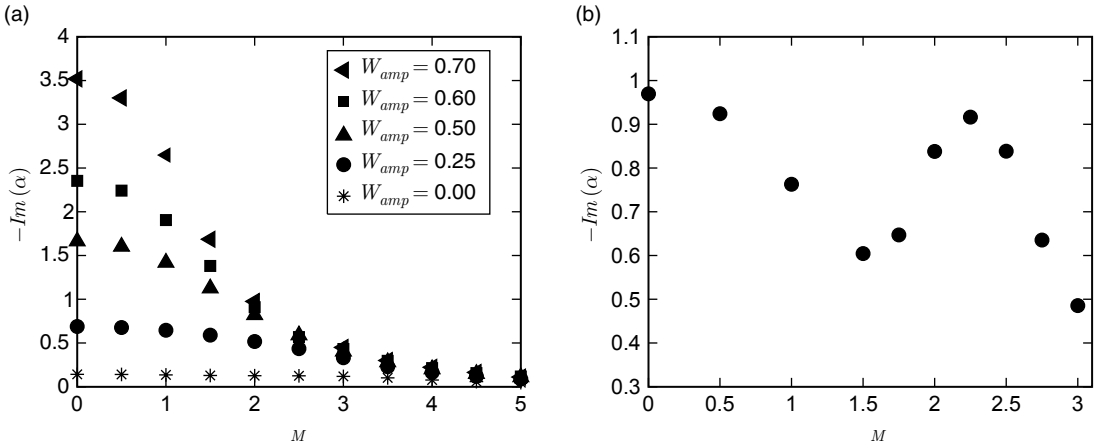

Figure 8. Influence of Mach number on the the maximum growth rates of (a). Shear Layer Mode I and (b). Wake Mode I.

effect of compressibility. This is apparent from the fact that, on increasing Mach number, even for wake deficit as high as W_{amp} = 0.7 the maximum growth rate of Shear Layer Mode I monotonically approaches zero. For Wake Mode II (see Fig. 8b) different ranges of Mach numbers show different trends in the growth rate. Starting from M = 0 and increasing Mach number up to 1.5, reduces the maximum growth rate. Increasing Mach number above 1.5, up to 2.25, increases the maximum growth rate. Beyond M = 2.25 the growth rate starts to fall off.

4. HEATED JETS

We now examine the stability of heated jets by varying the temperature ratio $\frac{T_{01}}{T_\infty}$ for the profile with W_{amp} = 0.7 at Mach numbers 0.5 and 1.

Figure 9 shows profiles of static temperatures for different temperature ratios $\frac{T_{01}}{T_\infty}$ at a Mach number of 1. Note that these temperature profiles are obtained by applying the Crocco equation 21, on the velocity profile with W_{amp} = 0.7 shown in Fig. 2a. Note that for the present analysis we consider both the primary jet and the secondary jet to have same stagnation temperature.

Figure 10 shows the influence of the temperature ratio $\frac{T_{01}}{T_\infty}$, at Mach numbers of 0.5 and 1, on the growth rates for various stability modes. In Fig. 10a one can see that, for Shear Layer Mode I, increasing the temperature ratio reduces maximum growth rates for both Mach numbers, i.e., 0.5 and 1.0. As far as the range of unstable frequencies is concerned, it increases upon heating the jet. The aforementioned observations in the context of Shear Layer Mode I, apply to Shear Layer Mode II (refer Fig. 10b) too. Figure 10c shows that for Wake Mode I, the growth rate trends with respect to the heating of the jet are complicated. We will elaborate on them in detail while explaining Fig. 12. In Fig. 11 one can see that heating the jet always increases the phase speed, irrespective of the Mach number and type of the stability mode.

We now examine of the maximum growth rate of Wake Mode I for different Mach number across a range of temperature ratio $\frac{T_{01}}{T_\infty}$ = {1, 1.5, 2}. In Fig. 12 one can see that upon increasing the temperature ratio, the maximum growth rate peaks at a certain temperature ratio, and then falls off. The temperature ratio at which the maximum growth rates peaks depends on the particular Mach number. For the range of Mach numbers and temperature ratios tested, one can see that upon increasing the Mach number, both the temperature ratio at which the maximum growth rate peaks and the maximum growth rate itself reduces.

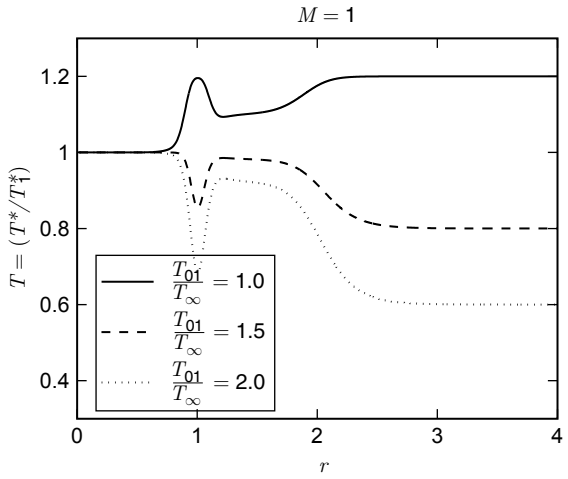

Figure 9. Static temperature distribution of the velocity profile W_{amp} = 0.7 shown in Fig. 2a for different temperature ratios $\frac{T_{01}}{T_\infty}$ at $M = 1$.

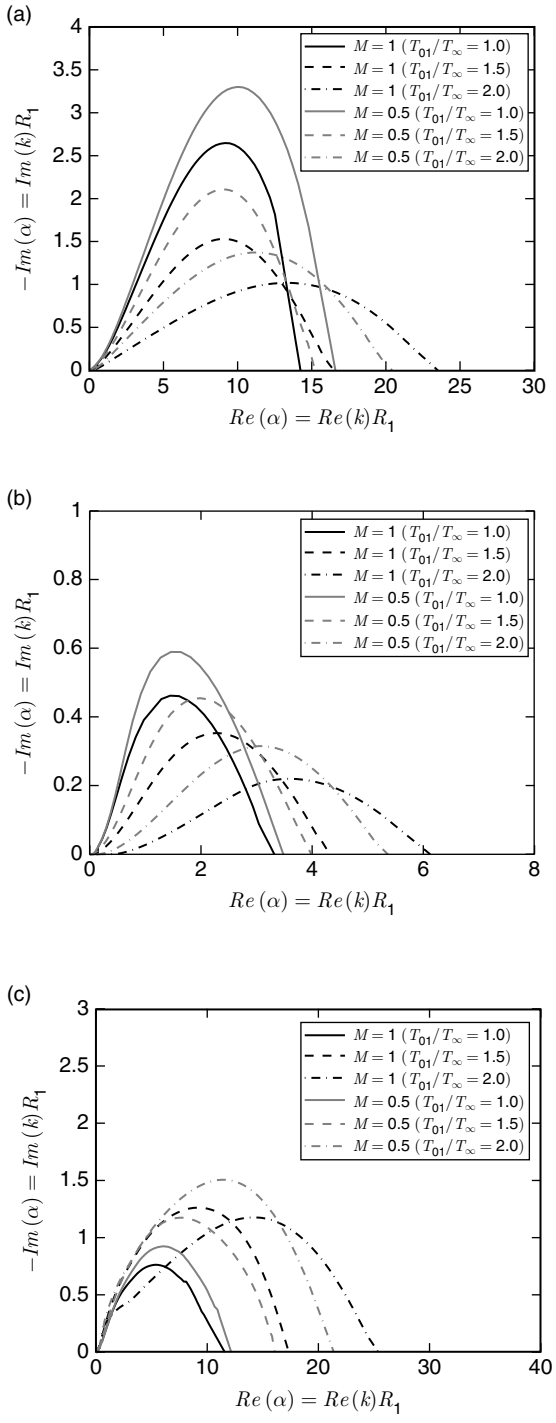

Figure 10. Influence of temperature ratio $\left(\frac{T_{01}}{T_\infty}\right)$ on the spatial growth rate of (a) Shear Layer Mode I; (b) Shear Layer Mode II and (c) Wake Mode I.

We now shift our focus to the helical modes, i.e., n = 1. We compare the stability characteristics of the helical mode with that of the axisymmetric mode for different values of W_{amp}. We do this comparison for all the three radial modes, viz., Shear Layer Mode I (Fig. 13), Shear Layer Mode II (Fig. 14) and Wake Mode I (Fig. 15). As apparent from these figures the influence of the azimuthal wavenumber on the stability characteristics of the radial modes is marginal.

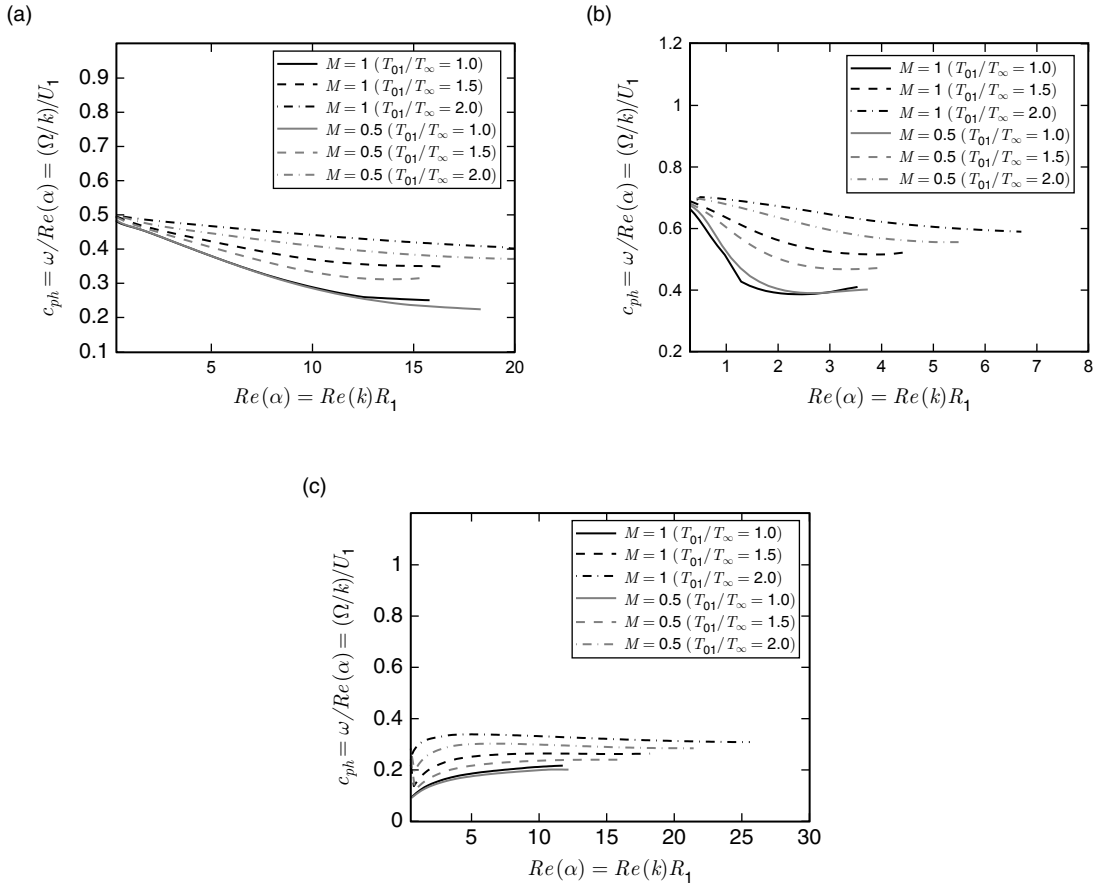

Figure 11. Influence of temperature ratio $\left(\frac{T_{01}}{T_\infty}\right)$ on the spatial phase velocity rate of (a) Shear Layer Mode I; (b) Shear Layer

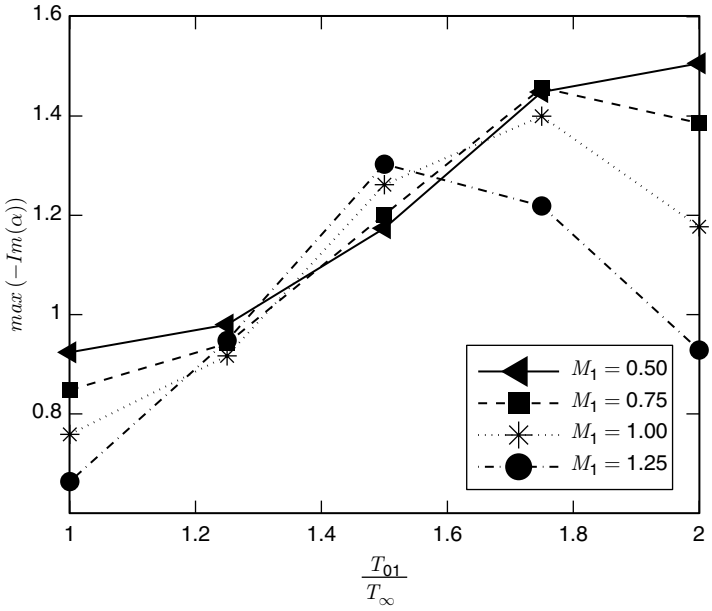

Figure 12. Influence of temperature ratio $\frac{T_{01}}{T_\infty}$ at different Mach numbers on the maximum growth rates of Wake Mode I.

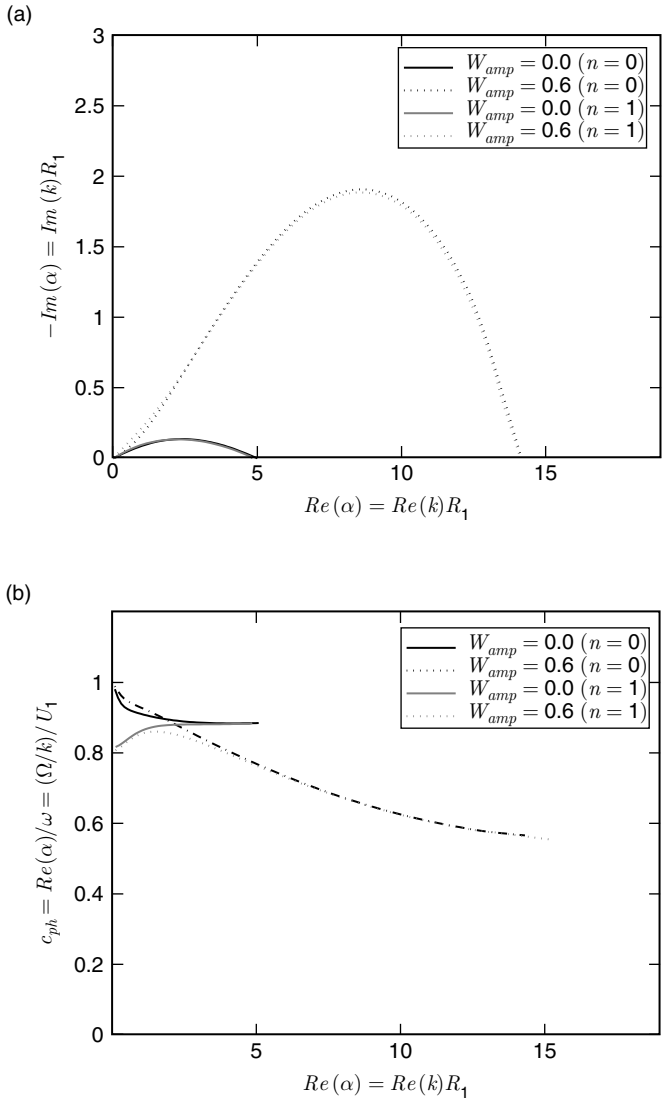

Figure 13. Comparison between axisymmetric (n = 0) and helical mode (n = 1), for Shear Layer Mode I, for different values of W_{amp} (a) spatial growth rates; (b) phase velocities.

5. RADIATING MODES

In the frame of reference of the instability waves, if both the the primary jet and the secondary jet are supersonic, then such instability waves are referred to as the supersonic mode. Mathematically this is equivalent to $M_{c1} > 1$ and $M_{c2} > 1$. Here M_{c1} is convective Mach number of the instability wave of the primary jet and M_{c2} is convective Mach number of the instability wave of the secondary jet. Definitions of these convective Mach numbers are given in Equation (23). Eigenfunctions associated with the supersonic modes persist several diameters away from the inflection points, unlike Kelvin Helmholtz instabilities for which pressure perturbations are mainly situated across the inflection point. Having direct relevance for the aeroacoustics, these modes are sometimes referred to as radiating modes.

Following the work of Fang and Reshotko [16] we now derive a criterion, in terms of phase velocities c_{ph1} and c_{ph2} of the instability waves, for the existence of the radiating supersonic modes. Here c_{ph1} and c_{ph2} refer to the phase velocity of the instability waves, with respect to the primary jet and the secondary jet respectively. Convective Mach numbers M_{c1} and M_{c2} of the instability waves, with respect to the primary jet and the secondary jet respectively, are as follows.

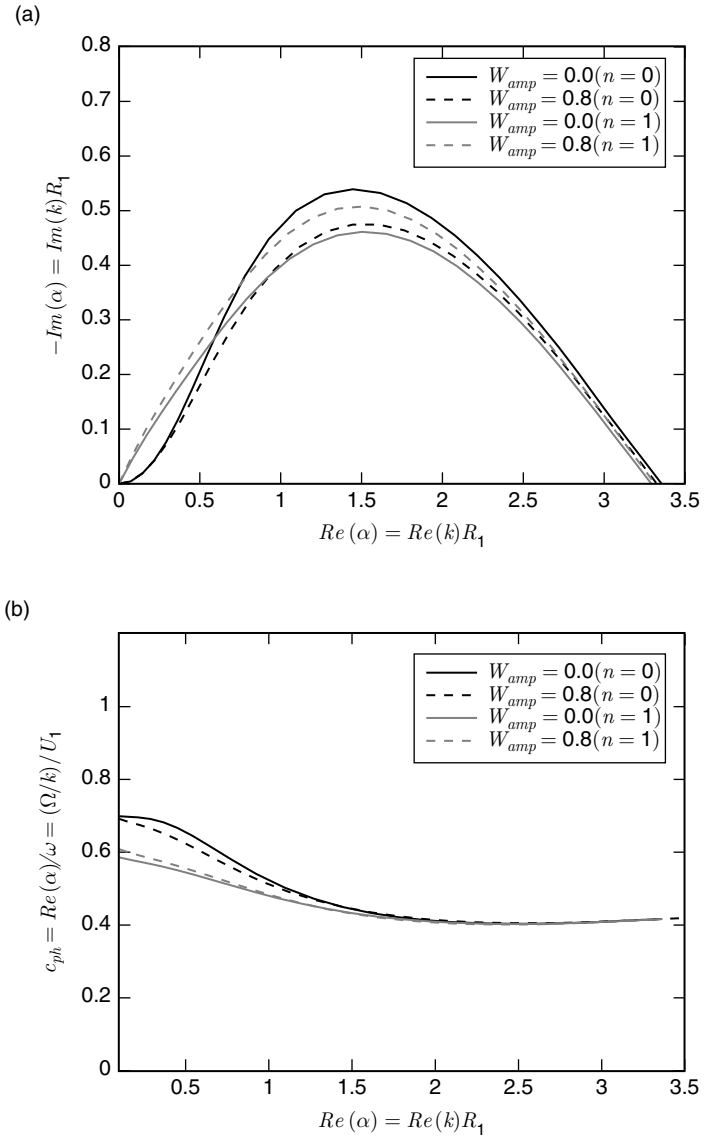

Figure 14. Comparison between axisymmetric (n = 0) and helical mode (n = 1), for Shear Layer Mode II, for different values of W_{amp}. (a) spatial growth rates; (b) phase velocities.

$$M_{c1} = (1 - c_{ph1})M_1, M_{c2} = M_1 \frac{c_{ph2} - h}{\sqrt{\kappa}} \tag{23}$$

where,

$$\kappa = \frac{T_2^*}{T_1^*} = \frac{1}{2}(\gamma - 1)h(1-h)M_1^2 + h + \frac{T_\infty}{T_1}(1-h) \tag{24}$$

For

$$M_{c1} = 1 \Rightarrow (c_{ph1})_{critical} = 1 - \frac{1}{M_1}, M_{c2} = 1 \Rightarrow (c_{ph2})_{critical} = h + \frac{\sqrt{\kappa}}{M_1} \tag{25}$$

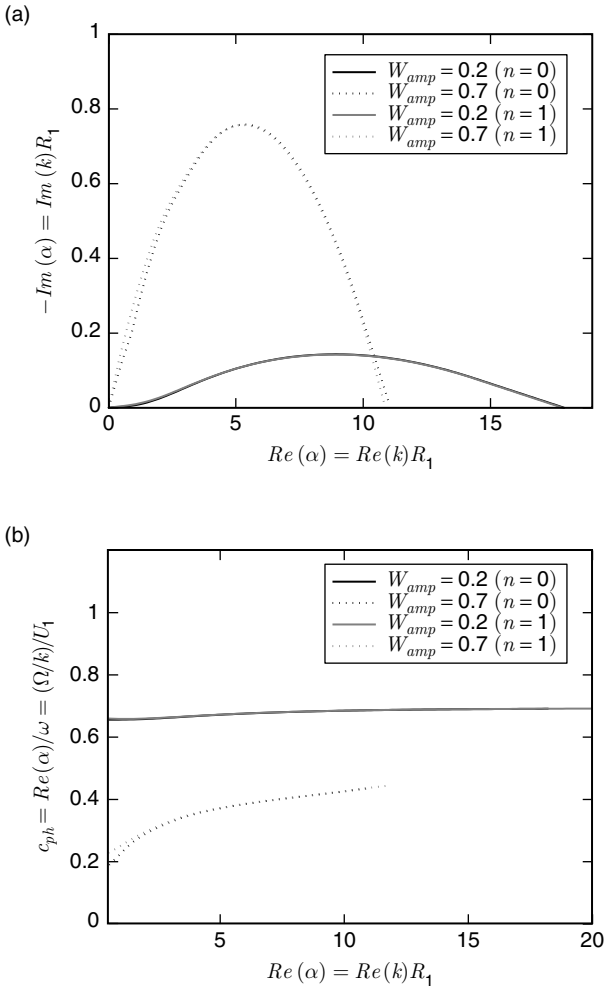

Figure 15. Comparison between axisymmetric (n = 0) and helical mode (n = 1), for Wake Mode I, for different values of W_{amp} (a) spatial growth rates; (b) phase velocities.

The condition for the radiating supersonic modes is

$$(c_{ph2})_{critical} < c_{ph} < (c_{ph1})_{critical} \tag{26}$$

Figure 16a represents this condition graphically. It is only when the phase velocity of the instability waves lies within the area enclosed by the curves $(c_{ph1})_{critical}$ and $(c_{ph2})_{critical}$, that the instability waves can radiate. Figure 16b represents $(c_{ph1})_{critical}$ and $(c_{ph2})_{critical}$ for different velocity ratios 'h' and temperature ratios '$\frac{T_{01}}{T_\infty}$'. As one can see for h = 0.7 and for $\frac{T_{01}}{T_\infty}$ = 1 and $\frac{T_{01}}{T_\infty}$ = 1.5, for the range of Mach numbers considered there exists no radiating mode.

6. CONCLUDING REMARKS

Coannular jet velocity profiles without any wake component in them, typically show only two instability modes, viz., one associated with the inflection point in the shear layer between primary jet and secondary jet (referred to as Shear Layer Mode I in the present paper) and the other one associated with the inflection point in the shear layer between the secondary jet and the ambient (referred to as

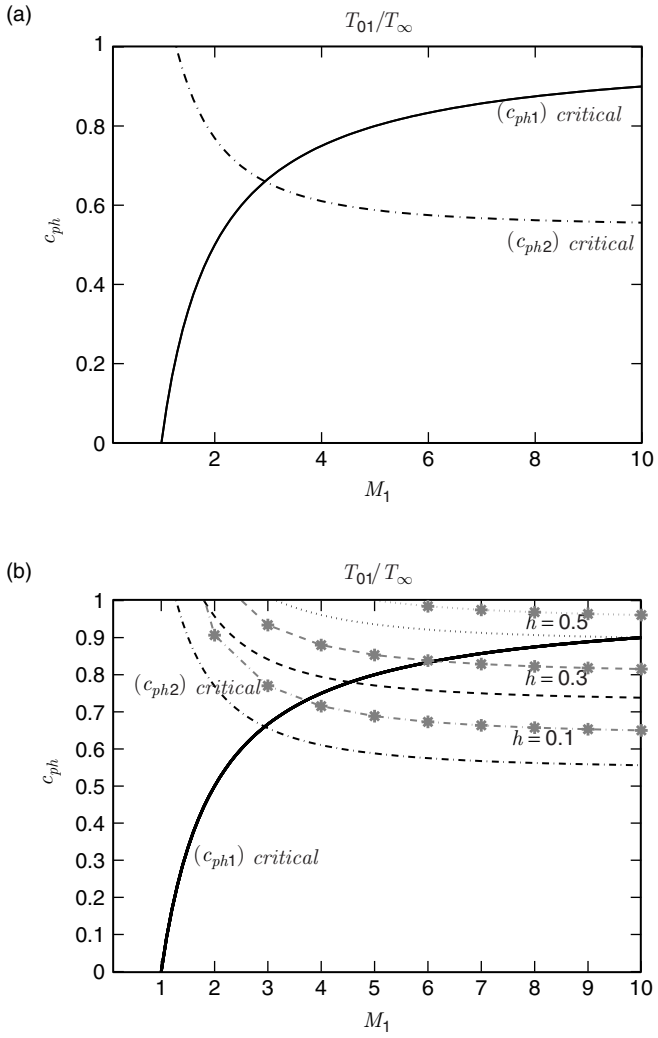

Figure 16. Convective phase velocity criterion, (a) illustration of the criterion for radiating supersonic modes; (b) critical phase velocities $(c_{ph1})_{critical}$ and $(c_{ph2})_{critical}$ for the different values of h. The black lines and grey lines with asterisk symbols represent cold jets and hot jets with $\frac{T_{01}}{T_\infty}$ = 1 and $\frac{T_{01}}{T_\infty}$ = 1.5 respectively.

Shear Layer Mode II in the present paper). Introduction of the wake in the shear layer between the primary jet and the secondary jet introduces an additional instability mode, i.e., Wake Mode I. To investigate the influence of the inner nozzle wake on the stability characteristics of these different instability modes, a compressible Rayleigh flow solver, using a shooting method, in radial coordinates has been developed. For better computational performance, the solver incorporates the phase velocity formulation to find the solution in wavenumber.

The key findings from the present work are as follows.

1. For radial mixing layers, formed downstream of the inner nozzle, the destabilization effect of the wake is not strong enough to counteract the stability effect due to compressibility. For the synthetic profiles tested in the present study, upon increasing the Mach number the growth rates always approached zero monotonically.
2. Heating the jets is found to stabilize both the shear layer instabilities mentioned in this work. As far as the wake instability is concerned the trend is non-monotonic. For small temperature ratios, the maximum growth rate of Wake Mode I increase, whereas for higher temperature ratio it decreases.

In addition several other observations were made:

1. For a given Mach number, increasing the wake deficit increases the maximum growth rate of Shear Layer Mode I and Wake Mode I, whereas it marginally reduces the growth rates of Shear Layer Mode II.
2. Apart from the shape of the eigenfunction, the trend in the phase velocities, is one of the other features that distinguishes the wake mode from the shear layer mode.
3. Changing the azimuthal mode number from $n = 0$ to $n = 1$ brings negligible changes to the stability characteristics to any of the three modes.
4. All findings mentioned above, except the one with respect to the compressibility effect, are consistent with trends observed for planar shear layers formed downstream of the splitter plate. For planar shear layers the presence of the wake of the splitter plate counteracts the stabilization effect provided by compressibility. As the convective Mach number exceeds unity, the presence of the wake increases the growth rate of the shear layer mode [2].

REFERENCES

[1] K. Viswanathan, L. T. Clark, and W. A. Seattle. Effect of nozzle internal contour on jet aeroacoustics. In *42nd AIAA Aerospace Sciences Meeting & Exhibit, Reno, NV,* Newport Beach, CA, USA, 2004. American Institute of Aeronautics and Astronautics.

[2] Mei Zhuang and Paul E. Dimotakis. Instability of wake-dominated compressible mixing layers. *Physics of Fluids,* 7(10): 2489–2495, October 1995.

[3] P. J Morris. The instability of high speed jets. *International Journal of Aeroacoustics,* 9(1): 150, 2010.

[4] A. Michalke. Survey on jet instability theory. *Progress in Aerospace Sciences,* 21: 159–199, 1984.

[5] H. Oertel. Mach wave radiation of hot supersonic jets. *Mechanics of sound generation inflows,* pages 275–281, 1979.

[6] C. Tam and F. Hu. On the three families of instability waves of high-speed jets. *Journal of Fluid Mechanics,* 201: 447483, 1989.

[7] P. Panickar and G. Raman. Criteria for the existence of helical instabilities in subsonic impinging jets. *Physics of Fluids,* 19: 106103, 2007.

[8] P. Panickar and G. Raman. Using Linear Stability Analysis as a Tool to Evaluate Jet and Cavity Flow Control Situations. *International Journal of Flow Control,* 1(1): 43–72, 2009.

[9] Brian S. Thurow, Naibo Jiang, Jin-Hwa Kim, Walter Lempert, and Mo Samimy. Issues with measurements of the convective velocity of large-scale structures in the compressible shear layer of a free jet. *Physics of Fluids,* 20(6): 066101, 2008.

[10] B. Thurow, M. Samimy, and W. Lempert. Compressibility effects on turbulence structures of axisymmetric mixing layers. *Physics of Fluids,* 15: 1755, 2003.

[11] E. Villermaux and H. Rehab. Mixing in coaxial jets. *Journal of Fluid Mechanics,* 425: 161185, 2000.

[12] H. Rehab, E. Villermaux, and E. J. Hopfinger. Flow regimes of large-velocity-ratio coaxial jets. *Journal of Fluid Mechanics,* 345: 357381, 1997.

[13] W. J.A Dahm, C. E Frieler, and G. Tryggvason. Vortex structure and dynamics in the near field of a coaxial jet. *J. Fluid Mech,* 241: 371402, 1992.

[14] M. D. Dahl and P. J. Morris. Noise from supersonic coaxial jets, part 1: Mean flow predictions. *Journal of Sound and Vibration,* 200(5): 643663, 1997.

[15] M. D. Dahl and P. J. Morris. Noise from supersonic coaxial jets, part 2: normal velocity profile. *Journal of Sound and Vibration,* 200(5): 665699, 1997.

[16] Y. C Fang and E. Reshotko. Inviscid spatial stability of a developing supersonic axisymmetric mixing layer. *AIAA journal,* 37(1): 2328, 1999.

[17] A. Michalke. On the influence of a wake on the inviscid instability of a circular jet with external flow. *European journal of mechanics. B, Fluids,* 12: 579–595, 1993.

[18] D. Perrault-Joncas and S. A Maslowe. Linear stability of a compressible coaxial jet with continuous velocity and temperature profiles. *Physics of Fluids,* 20: 074102, 2008.

[19] H. Schlichting, K. Gersten, and K. Gersten. *Boundary-layer theory.* Springer Verlag, 2000.

[20] S. A Ragab and J. L. Wu. Linear instabilities in two-dimensional compressible mixing layers. *Physics of Fluids A: Fluid Dynamics,* 1: 957, 1989.

[21] N. D. Sandham and W. C. Reynolds. Compressible mixing layer- linear theory and direct simulation. *AIAA journal,* 28(4): 618624, 1990.

[22] D. Papamoschou and A. Roshko. The compressible turbulent mixing layer: an experimental study. *J. Fluid Mech,* 197: 453–477, 1988.